Structural and effective brain connectivity underlying biological motion detection

Arseny A. Sokolov[a,b,c,1], Peter Zeidman[b], Michael Erb[d], Philippe Ryvlin[a], Karl J. Friston[b], and Marina A. Pavlova[e]

[a]Service de Neurologie, Département des Neurosciences Cliniques, Centre Hospitalier Universitaire Vaudois, 1011 Lausanne, Switzerland; [b]Wellcome Centre for Human Neuroimaging, Institute of Neurology, University College London, WC1N 3BG London, United Kingdom; [c]Neuroscape Center, Department of Neurology, University of California, San Francisco, CA 94158; [d]Department of Biomedical Magnetic Resonance, University of Tübingen Medical School, 72076 Tübingen, Germany; and [e]Department of Psychiatry and Psychotherapy, University of Tübingen Medical School, 72076 Tübingen, Germany

Edited by Peter L. Strick, University of Pittsburgh, Pittsburgh, PA, and approved October 30, 2018 (received for review August 2, 2018)

The perception of actions underwrites a wide range of socio-cognitive functions. Previous neuroimaging and lesion studies identified several components of the brain network for visual biological motion (BM) processing, but interactions among these components and their relationship to behavior remain little understood. Here, using a recently developed integrative analysis of structural and effective connectivity derived from high angular resolution diffusion imaging (HARDI) and functional magnetic resonance imaging (fMRI), we assess the cerebro-cerebellar network for processing of camouflaged point-light BM. Dynamic causal modeling (DCM) informed by probabilistic tractography indicates that the right superior temporal sulcus (STS) serves as an integrator within the temporal module. However, the STS does not appear to be a "gatekeeper" in the functional integration of the occipito-temporal and frontal regions: The fusiform gyrus (FFG) and middle temporal cortex (MTC) are also connected to the right inferior frontal gyrus (IFG) and insula, indicating multiple parallel pathways. BM-specific loops of effective connectivity are seen between the left lateral cerebellar lobule Crus I and right STS, as well as between the left Crus I and right insula. The prevalence of a structural pathway between the FFG and STS is associated with better BM detection. Moreover, a canonical variate analysis shows that the visual sensitivity to BM is best predicted by BM-specific effective connectivity from the FFG to STS and from the IFG, insula, and STS to the early visual cortex. Overall, the study characterizes the architecture of the cerebro-cerebellar network for BM processing and offers prospects for assessing the social brain.

biological motion | dynamic causal modelling | diffusion tensor imaging | functional MRI | network analysis

Nonverbal social cognition (inferring the intentions and affective and mental states of others based on nonverbal information) predominates in our daily life (1–3). Understanding of bodily expressions represents a key element of social cognition (3–5). Perception of dynamic bodily signals is commonly assessed by point-light biological motion (BM; ref. 6), as it enables one to separate the effects of motion from other attributes such as body shape or facial expressions (Fig. 1). Innate tuning to body motion is seen across species (7, 8). Studies using different imaging modalities, such as functional magnetic resonance imaging (fMRI), positron emission tomography, electroencephalography (EEG), and magnetoencephalography, have unveiled components of the BM processing network. However, communication within this network remains little understood.

The main foci of reported activation are the superior temporal sulcus (STS; refs. 9–19), fusiform gyrus (FFG; refs. 16 and 20–22), middle temporal cortex (MTC; refs. 11 and 20), parietal regions (10, 17, 21, 23), inferior frontal gyrus (IFG; refs. 14 and 24), bilateral insula (14, 25), and the left lateral cerebellum (26). More recently, by using whole-head ultra-high-field 9.4T fMRI and temporal analysis of blood oxygen level-dependent (BOLD) responses, distinct large-scale ensembles of regions (including early visual areas, the precuneus, several temporal and parietal regions, and the right IFG) have been reported to play in unison during different stages of BM processing (27).

The only task-related functional connectivity study of BM processing suggests that the right FFG, MTC, and STS are functionally integrated and that the right STS exclusively entertains connectivity with the right insula and IFG (28). These findings may speak to a right temporal BM processing module comprising the FFG, MTC, and STS. Furthermore, they imply a "gatekeeper" role for the STS. This means that the STS receives preprocessed information from the FFG and MTC, but is the only region in communication with higher-order brain areas. This agrees with the current conceptualization of the STS as the cornerstone of the BM processing network (3, 15). However, the role of the FFG and MTC in BM processing remains unclear. The FFG exhibits strong responses not only to faces but also to static and dynamic bodies, leading to a designation of fusiform face and body areas (20, 29, 30). The MTC harbors both V5/MT+, crucial for global motion processing (31), and the extrastriate body area, preferentially activated by bodies (32). Even the V5/MT+ is reported to be specifically tuned to body parts compared with objects (33).

Here, we assessed how BM processing modulates the causal interactions within the temporal module to infer the pattern of connectivity among the FFG, MTC, and STS. Second, we evaluated whether BM modulates the FFG and MTC outputs to the STS solely (i.e., a "gatekeeper" architecture) or also the FFG/MTC effective connectivity with other higher-order regions, thus indicating functional roles of the FFG and MTC beyond preprocessing for the STS. Finally,

Significance

Visual perception of body motion is of substantial value for social cognition and everyday life. By using an integrative approach to brain connectivity, the study sheds light on architecture and functional principles of the underlying cerebro-cerebellar network. This circuity is organized in a parallel rather than hierarchical fashion. This may explain why body-language reading is rather resilient to focal brain damage but severely affected in neuropsychiatric conditions with distributed network alterations. Furthermore, visual sensitivity to body motion is best predicted by specific top-down feedback to the early visual cortex, as well as functional communication (effective connectivity) and presence of white-matter pathways between the right fusiform gyrus and superior temporal sulcus. The findings allow better understanding of the social brain.

Author contributions: A.A.S., M.E., K.J.F., and M.A.P. designed research; A.A.S. and M.E. performed research; A.A.S., P.Z., and K.J.F. contributed new reagents/analytic tools; A.A.S., M.E., and M.A.P. analyzed data; A.A.S., P.Z., P.R., K.J.F., and M.A.P. wrote the paper; and A.A.S., P.Z., P.R., K.J.F., and M.A.P. contributed to data interpretation.

The authors declare no conflict of interest.

This article is a PNAS Direct Submission.

[1]To whom correspondence should be addressed. Email: arseny.sokolov@chuv.ch.

This article contains supporting information online at www.pnas.org/lookup/suppl/doi:10.1073/pnas.1812859115/-/DCSupplemental.

Published online December 4, 2018.

Fig. 1. Illustration of point-light biological motion. Dots (here, in orange) are placed on the major joints of a walking person crossing the marketplace in the medieval downtown of Tübingen. Only the moving point-lights against a dark background are retained as experimental stimuli. The arty image was created by M.A.P.

inspired by our recent findings (27, 34), we asked whether the early visual cortex receives BM-specific top-down modulation from higher-order regions.

We used Dynamic Causal Modelling (DCM), the most established approach for effective connectivity analysis available for fMRI and magnetoencephalography/EEG (35, 36). While functional connectivity between two regions may be inferred due to their coactivation, even in the absence of causal interactions, effective connectivity represents causal coupling among brain areas (37). Recent psychophysiological interaction (PPI) work in autism spectrum disorder (ASD) reported that effective connectivity between the medial prefrontal cortex and right STS is related to the visual sensitivity to BM (38). Effective connectivity between the STS and lateral cerebellum was linked to social impairments in ASD (39). Both PPI and DCM allow one to assess the modulation of effective connectivity by task context, but DCM additionally provides information on directionality (35). So far, only two DCM studies have addressed BM processing and were limited to specific connections: The right STS has been shown to entertain reciprocal effective connectivity with the left lateral cerebellar lobule Crus I (26) and the right FFG (40). As interregional communication depends on interconnecting white-matter pathways, we hypothesized our understanding of BM processing would benefit from a more comprehensive network characterization. This approach assimilates white-matter connectivity as measured by high angular resolution diffusion imaging (HARDI) with effective connectivity derived from fMRI. This analysis is afforded by our recently developed structurally informed parametric empirical Bayes (si-PEB) method (41).

Our additional aim was to clarify whether, and, if so, how, network connectivity predicts behavioral measures of performance. Most previous imaging studies have used canonical unmasked point-light BM displays that make the perceptual tasks relatively easy. Camouflaged BM, by affording reduced visual signal-to-noise ratio (*SI Appendix*, Fig. S1), rendered our BM task more demanding, thereby increasing variability in performance. The use of camouflaged BM in the present study enabled us to evaluate possible links between the visual sensitivity to BM and network connectivity.

Results

Behavior. Accuracy in recognition of presence and absence of the point-light walker (as percentage of correct responses) within an array of distractors was 90.3% (range 71.7–100%). The average hit rate (correct detection of walker-present trials) was 87.2% (range 71.7–100%). The group d-prime as a measure of the visual sensitivity to BM in the signal detection theory (42) was 3.64 ± 1.55 (range 1.15–6.43).

fMRI Analysis. Whole-brain analysis of the differential BOLD response for walker-present vs. walker-absent displays [represented by a positive parametric regressor in the general linear model (GLM); $P < 0.05$, family-wise error (FWE) corrected; Fig. 2] revealed BM-specific effects in the bilateral MTC [right: $x = 46$, $y = -68$, $z = 0$; left: $x = -48$, $y = -70$, $z = -2$; Montreal Neurological Institute (MNI) coordinates], right posterior STS ($x = 50$, $y = -40$, $z = 10$), FFG ($x = 42$, $y = -56$, $z = -14$), right anterior insula ($x = 36$, $y = 24$, $z = 2$), right IFG ($x = 46$, $y = 10$, $z = 32$), and the left cerebellar lobule Crus I ($x = -36$, $y = -54$, $z = -28$).

Integration of Structural and Effective Connectivity. For analysis of effective connectivity, DCMs including the right FFG, MTC, STS, insula, IFG, and the left lateral cerebellar lobule Crus I were created (*Materials and Methods* and Fig. 2*G*). A region in the early visual cortex [occipital cortex (OCC); $x = 18$, $y = -94$, $z = 0$] activated by both types of stimuli compared with baseline ($P < 0.05$, FWE corrected) was also included to provide a single, neurobiologically plausible entry point for the driving visual input.

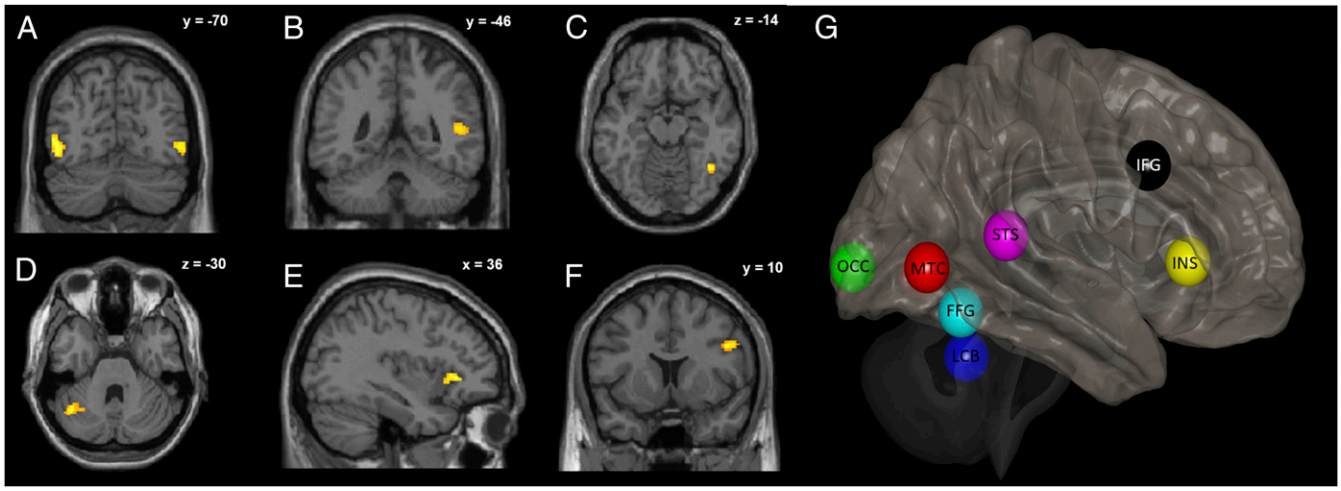

Fig. 2. Brain activity during perception of camouflaged BM. (*A–F*) Regions showing higher BOLD responses for walker-present compared with walker-absent displays ($P < 0.05$, FWE whole-brain corrected for multiple comparisons) are located in the bilateral MTC (*A*), right STS (*B*), right FFG (*C*), left lateral cerebellar lobule Crus I (LCB) (*D*), right anterior insula (INS) (*E*), and right IFG (*F*). Activation clusters are overlaid on the MNI T1 template, and slice positions in MNI space are provided in the right upper corner. (*G*) Location of the seven network nodes (including early visual cortex, OCC) used in probabilistic tractography and DCM. These nodes are overlaid on a 3D brain template.

Probabilistic tractography on the HARDI data returned the strengths of structural connections between these seven network nodes with the same coordinates and radius as specified for DCM. Subsequently, this structural connectivity was integrated in DCM constraining the group-level prior probability for the corresponding between-region effective connections in DCM. As the precise relationship between structural connection strength and prior probability can vary on a study-by-study basis (41), we created 405 different sigmoid mappings from structure to function defined by the hyperparameters α (intercept of the sigmoid), δ (sigmoid slope), and $\Sigma_{y\ max}$ (maximum prior second-level probability) and used Bayesian model reduction (43) to select the model with the greatest evidence (i.e., marginal likelihood).

The log evidence of the optimal structurally informed model ($\alpha = 0$, $\delta = 4$, and $\Sigma_{y\ max} = 0.5$; *SI Appendix*, Fig. S2*B*) relative to the uninformed model was 3.43, corresponding to a 97% posterior probability for the structurally informed model (with strong evidence in favor of one model concluded at a posterior probability of 95% or above; ref. 44). Direct structural pathways account for about two-thirds of effective connections within this network, particularly in the temporal module (connectivity between the MTC, FFG, and STS; *SI Appendix*, Fig. S2*D*).

Using this optimal model afforded by the si-PEB procedure (41), we tested three specific hypotheses on how BM modulates effective connectivity within distinct parts of the network: (*i*) the temporal module (*SI Appendix*, Fig. S3), (*ii*) its connections to the IFG and insula (*SI Appendix*, Fig. S4), and (*iii*) top-down connections to the early visual cortex (*SI Appendix*, Fig. S5). All variants of models under each hypothesis (i.e., sets of connections showing BM effects) were specified in terms of prior constraints on modulatory effects of BM, yielding 1,024 models. The evidence for the ensuing models was evaluated by using Bayesian model reduction (43) within and between each set. Subsequently, Bayesian model averaging was used to estimate BM-sensitive changes in effective connectivity throughout the network.

Modulation of Effective Connectivity by Biological Motion in the Temporal Module. First, we asked which connections in the temporal module, and, in particular, between the FFG on one side and the MTC and STS on the other, were selectively modulated by processing of camouflaged BM (*SI Appendix*, Fig. S3). Two equally probable models outperformed the remaining alternatives: model 12 ("only connections from the FFG to MTC and from the FFG to STS are modulated by BM"; family-wise posterior probability 48%) and model 11 ("only the connection from the FFG to STS is modulated by BM"; family-wise posterior probability 44%). Given the pattern of extrinsic connectivity (*SI Appendix*, Fig. S2*C*), we inferred an absence of effective connectivity from the STS and MTC to the FFG (Fig. 3*A*). Bayesian model averaging (followed by thresholding at a posterior probability of 95% or above) indicated that BM processing did not significantly modulate the ample baseline effective connection from the FFG to MTC nor the connection from the STS to MTC. Overall, these findings suggest that the STS receives BM-specific afferents from both the FFG and MTC, without substantial BM-specific feedback from the STS or cross-talk between the FFG and MTC. This is consistent with an integrator role of the STS in the temporal module.

Interplay of the Temporal Module with IFG and Insula. We further assessed whether the integrator role of the STS within the temporal module implicates a gatekeeper function (i.e., the STS exclusively directing temporal module output to higher-order regions such as the IFG and insula; *SI Appendix*, Fig. S4). To this end, we compared the evidence for models with exclusive BM-specific modulation of effective connectivity between the STS and IFG/insula with evidence for models where effective connections linking the IFG and insula with the MTC, FFG, and/or STS were also modulated. Bayesian model reduction clearly indicated that the optimal model was equipped with BM-specific modulation of all connections between the MTC, FFG, and STS on one hand and the IFG and insula on the other (model 1; family-wise posterior probability 100%). These results do not speak in favor of a gatekeeper role of the STS, but rather underline significant contributions of the FFG and MTC to the network. In parallel to the STS, both these areas exhibit BM-specific projections to higher-order regions.

Modulation of Top-Down Influences by Biological Motion Processing. Bayesian model reduction yielded a family-wise posterior probability of 100% for models in which BM modulates top-down connections from the IFG, insula, and STS to the early visual cortex (OCC; *SI Appendix*, Fig. S5). Bayesian model averaging indicated divergent profiles of modulation: BM processing had

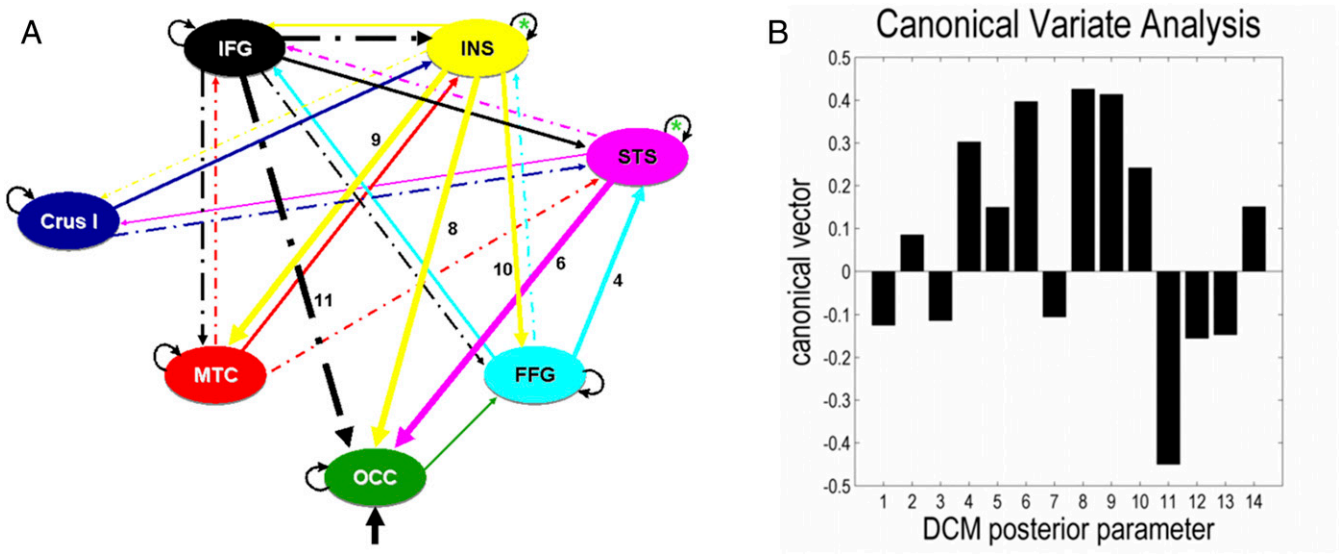

Fig. 3. Modulation of effective connections during BM processing—and relationship between BM-specific changes in connectivity and the visual sensitivity to BM. (*A*) Bayesian model averaging of changes in effective connectivity during visual processing of BM over the entire network. These results provided very strong evidence (posterior probability of a particular BM effect being present at or above 95%) that (*i*) effective connectivity from the MTC to STS and from the FFG to STS, but not between the FFG and MTC, was modulated by BM processing; (*ii*) reciprocal connections between the MTC/FFG and IFG/insula as well as between the STS and IFG, but not between the STS and insula were modulated by BM processing; and (*iii*) insula outputs were predominantly enhanced by BM, whereas BM processing exerted an inhibitory effect on IFG outputs. Both regions also exhibited BM-specific cross-talk. Furthermore, BM modulated the connection from the early visual cortex (OCC) to FFG (but not from the OCC to MTC), from the STS to OCC, and bidirectional connections between the left lateral cerebellar lobule Crus I and insula and between Crus I and STS (in different ways). Self-connections of the insula and STS (green asterisks) were also modulated by BM. Solid lines represent excitatory and dashed lines inhibitory effects, and arrow thickness corresponds to connection strength. Numbers designate the connections (defined by DCM posterior parameters) that best explain (as indicated by the canonical vector magnitude) the visual sensitivity to BM in a canonical variate analysis. (*B*) The relationship (characterized by canonical vectors) between 14 BM-specific DCM posterior parameters and the visual sensitivity to BM afforded by a canonical variate analysis ($P = 0.03$). Individual levels of BM modulation of top-down connections from the IFG to OCC (parameter 11), insula to OCC (8), insula to MTC (9), and STS to OCC (6) served as best predictors of individual visual sensitivity to BM (as measured by d-prime). Modulations of the connections from the FFG to STS (4) and from the insula to FFG (10) also played important roles. Only modulatory parameters within the model space spanned by our three hypotheses and with posterior probabilities at or above 95% at the group level were included in the canonical variate analysis.

excitatory effects on connections from the insula to OCC, MTC, and FFG and from the STS to OCC, whereas it had inhibitory effects on connections from the IFG to OCC, MTC, and FFG (Fig. 3*A*). Overall, this outcome suggests that the early visual cortex receives BM-specific top-down influences and may indicate differential contributions of the STS, insula, and IFG to the BM processing network.

Effective Connectivity Predicts Behavior. By using a canonical variate analysis, the relationship between BM-specific changes in effective connectivity and the visual sensitivity to BM was assessed at the between-subject level. This analysis included modulatory parameters that reached a posterior probability of 95% in Bayesian model averaging within the model space spanned by our hypotheses. The canonical variate analysis revealed a significant mapping between BM modulatory parameters and d-prime, an index of the visual sensitivity to BM ($P = 0.03$; Fig. 3*B*). The principal canonical vectors suggested that the visual sensitivity was best predicted by top-down effects from the IFG to OCC, the insula to OCC, the insula to MTC, and the STS to OCC (in descending order). Other strong predictors of the visual sensitivity to BM were the modulatory parameters on the connections from the FFG to STS and from the insula to FFG.

Structural Pathway Between the FFG and STS and Its Relationship to BM Detection. The group structural adjacency matrix derived from probabilistic tractography indicated white-matter connectivity between the FFG and STS (*SI Appendix*, Fig. S2*A*). At a single-subject level, significant structural connectivity (at 5% of the robust intensity range corresponding to a 95% confidence interval; ref. 45) was found in 5 of 12 participants (Fig. 4*A*). Participants with significant FFG-STS structural connectivity exhibited higher BM hit rates than subjects without significant connectivity (Mann–Whitney test $U = 0$; $P = 0.003$; two-tailed, effect size $r = 0.80$). In contrast, d-prime, a measure of the visual sensitivity to BM (that accounts for both hit and false alarm rates) did not significantly differ between the two groups ($U = 11$; $P > 0.05$). This white-matter pathway therefore appears to play a specific role in BM detection, but not in discrimination between noise and camouflaged BM.

Discussion

The integrative analysis of structural and effective connectivity and their relationship to behavior unveils several principles of functional integration within the network engaged in BM processing. The outcome confirms that the right STS plays an integrative role within the temporal module. However, involvement of the FFG and MTC in the BM network appears to go beyond mere preprocessing for the STS. Furthermore, the right STS, insula, and IFG exert substantial BM-specific top-down influences on the early visual cortex. The visual sensitivity to BM is best predicted by specific modulations of these top-down effective connections, as well as by structural and effective connectivity between the FFG and STS.

The Temporal BM Processing Module: All Roads Lead…to the STS? The right posterior STS is considered a cornerstone of the BM network (9–15, 17–19, 46–52). Consequently, the right STS has been put forward as an integrator within and between social brain networks (3). A recent analysis of functional connectivity

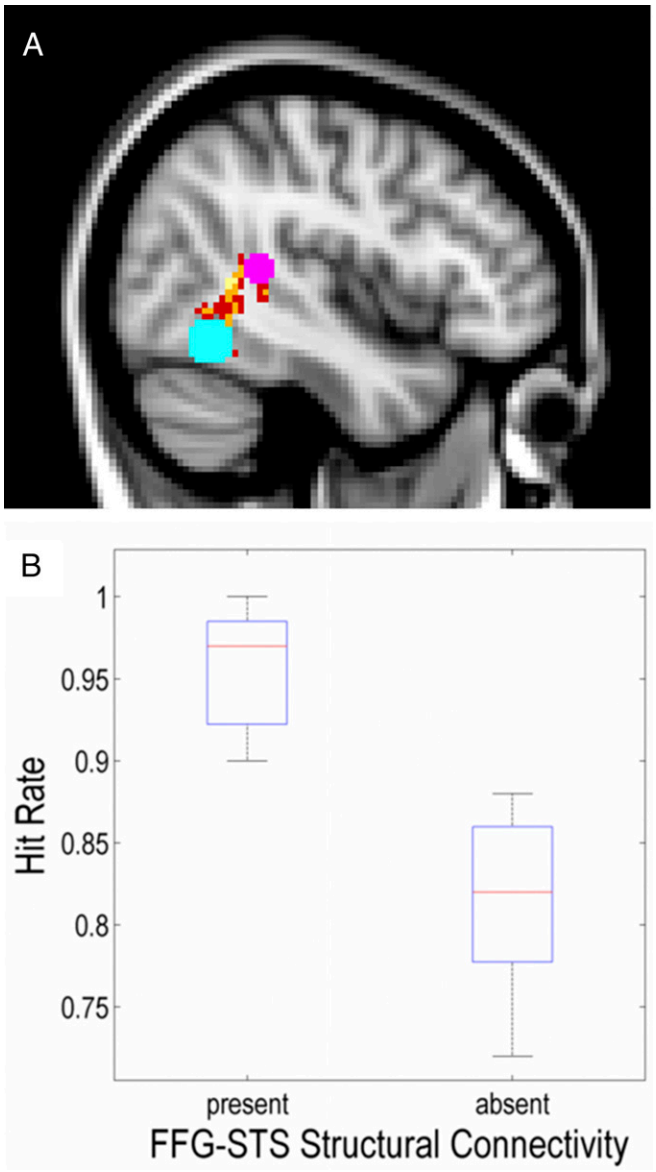

Fig. 4. White-matter pathway between the FFG and STS and relationship between prevalence of significant FFG–STS structural connectivity and detection of camouflaged BM. (*A*) The group variability map over probabilistic tractography outputs in five participants with significant pathways (at a threshold of 5% of the robust intensity range, corresponding to a confidence interval of 95%) between the STS (purple) and FFG (cyan) illustrates the trajectory of connecting fibers. (*B*) Subjects with significant structural connectivity between the FFG and STS (left boxplot) have a higher BM detection (hit) rate compared with subjects with nonsignificant FFG-STS connectivity (right boxplot; Mann–Whitney $U = 0$; $P = 0.003$). The median value of each group is represented by the red line. The top and bottom edges of the box indicate the 75th and 25th percentiles, respectively. The whiskers correspond to the highest and lowest hit rates in each group.

during various social perceptual tasks including BM processing supported this view (28). The present DCM analysis confirmed the integrative role of the STS in the temporal module, by indicating specific modulation of the effective connections from the FFG and MTC to the STS during BM processing.

The STS Is Not a Gatekeeper of the Temporal Module. Bayesian model comparison revealed BM-specific modulation of effective connectivity between the MTC and FFG on one hand and the IFG and insula on the other. The data thus indicate BM-specific contributions from the FFG and MTC to the entire network and do not support a gatekeeper function of the STS within the temporal module. Whereas previous research reported activation in the FFG and MTC during BM processing (11, 16, 20–22, 27), their contribution to the network underwriting BM detection remained largely unclear. Patient studies in relatively small groups of individuals with heterogeneous occipito-temporal lesions yielded controversial results as to the eloquence of these brain areas for BM processing (53, 54). One may speculate that the engagement of the FFG and MTC provides form-related information (55, 56), with the extrastriate body area in the MTC believed to be rather involved in the processing of body parts and the FFG in global body form representation (57, 58).

Pathway Between the FFG and STS Is Crucial for BM Detection. Significant associations between behavior on one side, and effective and structural connectivity on the other, point to a particular role of the pathway from the FFG to STS in BM processing. Previous research reported higher BOLD activation in both the STS and FFG accompanied by improvements in the visual sensitivity to camouflaged BM after training (16). Conclusions on effective (40, 59, 60) and structural connectivity (61–64) between the FFG and STS were mainly derived from research on face processing and remained controversial, in particular with respect to detection of a structural pathway. The present findings indicate one-way effective connectivity from the FFG to STS, with the strength of BM-specific modulation on this connection serving as a key predictor for the visual sensitivity to camouflaged BM.

Most important, corresponding structural connectivity was seen in about half of the participants. Given the orientation of the pathway perpendicular to the predominant fiber direction in this region (Fig. 4*A*), these insights may be attributable to the improved signal-to-noise ratio of the present HARDI dataset, related to the number of gradient directions and b values (65, 66). Moreover, the difference in BM detection (hit rate) between participants with and without measurable FFG-STS fiber pathways points to neurobiological plausibility of individual variability in structural connectivity (62, 63). Altered connectivity between the FFG and STS has been shown to contribute to deficient social perception in individuals with ASD (67). The present findings call for further investigation of the functional contribution of this connection to social cognition.

Top-Down Modulation of the Early Visual Cortex Matters. Strikingly, BM does not only modulate top-down connections from the IFG, insula, and STS to the FFG and MTC, but also to the early visual cortex (Fig. 3*A*). Furthermore, the strengths of these modulations are among the strongest predictors of the visual sensitivity to BM (Fig. 3*B*). Previous psychophysical work suggests that processing of camouflaged BM may depend on predictions (e.g., characteristic motion patterns) stored in hierarchically higher processing levels (68, 69). Inhibitory projections from the IFG, and excitatory projections from the STS and insula imply that these nodes may shape BM-specific network activity in different ways.

Under a predictive coding scheme (70), prediction errors in the early visual cortex (such as the discrepancy between predicted and sensed visual input) could be minimized by outputs from the IFG driving activity of inhibitory interneurons (71, 72). Conversely, reliability of sensory information may be enhanced by attentional mechanisms reducing the gain of inhibitory interneurons (73) through feedback from the STS and insula. Such top-down modulation of the early visual cortex is considered indispensable for selective attention (74) and, according to high-resolution 7T fMRI, mainly reaches superficial layers almost exclusively populated by inhibitory interneurons (75). The present

findings may indicate a more specific role of the early visual cortex in the network for BM processing than previously assumed. Ipsilateral and contralateral top-down projections to occipito-temporal areas may contribute to nonconscious BM processing in individuals with damage to the early visual cortex (76, 77).

The Lateral Cerebellum Interacts with Insula. The BM-specific top-down modulation by the right anterior insula may be related to its putative role as an interface of internal and external body awareness (78), also reflected in the implication of the insula in self-motion awareness (79, 80), imitation (81), the sense of agency (82), anosognosia for hemiparesis (83), and out-of-body illusions (84). Interestingly, the present study indicates that the left lateral cerebellar lobule Crus I also entertains effective connectivity loops with the insula (albeit without evidence for underlying direct structural connectivity) and not only with the STS as previously shown (26). In keeping with an overarching functional hypothesis for the cerebellum (85), the higher-level BM-specific predictions may be fine-tuned by the cerebellum, potentially having subsequent modulatory effects on the entire network via the cortical regions' distributed projections.

Network Approaches Bear Clinical Implications. Clinical evidence for the eloquence of single brain regions in BM perception is sparse, apart from the parieto-occipital white matter (86), IFG, areas adjacent to the parieto-temporal junction (24), and the left lateral cerebellum (87). This relative lack of consistent findings may be due to methodological factors such as heterogeneity of focal lesions and sample size, but may also indicate parallel instead of strictly hierarchical processing of BM. Parallel processing, as demonstrated in the present study, would be consistent with reports of altered visual sensitivity to BM in neuropsychiatric conditions such as autism (88–90) or schizophrenia (91–93), which are associated with more distributed network alterations (94, 95). Indeed, the local efficiency of intrinsic functional networks derived from resting-state fMRI data are related to behavioral variability in BM perception in typically developing participants (96).

In autistic children, fMRI activation for intact compared with scrambled BM in the social brain (including the STS, FFG, amygdala, and insula) predicts the efficacy of social communication interventions (97). The social value of BM is further underlined by reduced visual preference to BM in newborns with high familial risk of autism as opposed to those with a low risk (98). Inclusion of neuroimaging in studies of patients with focal lesions and neuropsychiatric conditions (99, 100) along with integrative network-level analyses such as those implemented in this study may afford a better understanding of aberrant social cognition that could inform clinical care.

Moreover, the methodological approach and data presented here may further promote investigation of the networks for body language reading, as well as their variability (3, 5, 101, 102). Among other factors, gender, presence of neuropsychiatric conditions, and the body language content itself may affect the decoding of intentions and emotions from dynamic point- and full-light bodily stimuli (103–109). Previous data indicate the STS and IFG may be engaged in inferring emotion and personality traits from point-light BM (110, 111). In both typically developing and autistic adults, a positive correlation was found between accuracy in emotion recognition from point-light BM and activity within the right STS (112). In male observers, same-gender full-light BM expressing threat activates a neural circuitry rather similar to the one reported here (104). However, the conceptualization of the networks involved in body language reading remains incomplete. Integrative analyses of structural and effective connectivity and their association to behavior may bridge this gap and shed light on interactions between the cerebro-cerebellar circuitry for BM processing and limbic structures.

Conclusions

In summary, the present integrative analysis of structural and effective connectivity suggests that the network for BM processing is organized in a parallel rather than hierarchical manner. This organization of the BM network appears neurobiologically plausible and aligns with recent experimental evidence and conceptual considerations challenging the traditional view of a strictly hierarchical organization of visual processing (113–115). The data highlight the significance of top-down modulations by the insula, STS, and IFG, as well as the pathway from the FFG to STS for veridical processing of BM. This work may inform future patient studies addressing the relationship between network pathology, deficient BM processing, and associated aberrations in social cognition.

Materials and Methods

Participants and Experimental Procedures. Fifteen right-handed, typically developing male subjects (age 26.0 ± 1.04 y) were studied, with normal visual acuity. None had a history of neurological or psychiatric conditions or regular drug intake (medication). The group of participants overlapped with that in previous studies on noncamouflaged BM (26, 116). The fMRI and HARDI data have been used for a methodological illustration of the si-PEB analysis of structural and effective connectivity (41) implemented in the present study. Two subjects had to be discarded from data analysis because of technical problems with stimulus presentation and another one because of failure to follow instructions. Recruitment of participants of the same gender and handedness ensured a homogenous group and thus avoided potential confounds. For example, handedness has been reported to influence lateralization of static face and body processing (117). Hemodynamic response in females fluctuates with menstrual cycle (118), and both hemodynamic and neuromagnetic brain responses to BM appear to be sex-specific (119, 120). The study was approved by the local Ethics Committee of the University of Tübingen Medical School, Germany. Subjects provided informed written consent and received financial compensation for study participation.

The camouflaged point-light BM displays (*SI Appendix*, Fig. S1) were inspired by a previous neuroimaging study (18). In brief, the stimuli consisted of a human walker represented by 11 bright dots on the head and main joints of the body, facing to the right and moving without translation, with a walking speed of ∼48 cycles per minute and each walking cycle lasting 62 frames (frame duration 20 ms). The point-light walker was simultaneously masked by 33 additional bright moving dots, created by random spatial distribution of three sets of the 11 dots comprising the original walker configuration on the screen, thereby preserving motion characteristics, size, and luminance of the dots. The other stimulus type was a walker-absent display matching the spatial density of the walker-present stimuli, consisting of four scrambled walker sets (in total, 44 dots). Cutting's algorithm (121) was used to create the stimuli, and the software Presentation (Neurobehavioral Systems Inc.) was used to display them. The stimuli were projected onto a screen outside the MRI scanner to be seen by the participants through a tilted mirror installed on the head coil. They subtended a visual angle of ∼12° vertically and 18° horizontally. Each stimulus was presented for 1,000 ms, interleaved with a fixation cross (also during rest). In a two-alternative forced-choice paradigm, participants had to decide on each trial whether a walker was present or absent, pressing the respective button with their right index finger (with the button order counterbalanced between participants).

MRI Recording and Analysis. A 3T scanner (TimTrio; Siemens Medical Solutions; 12-channel head coil) was used for data acquisition. A 3D T1-weighted magnetization-prepared rapid gradient echo [MPRAGE; 176 sagittal slices, repetition time (TR) = 2,300 ms, echo time (TE) = 2.92 ms, inversion time (TI) = 1,100 ms, voxel size = 1 × 1 × 1 mm^3] dataset served as anatomical reference. After field-map acquisition, two echo-planar imaging (EPI) sessions (114 volumes, 56 axial slices, TR = 4,000 ms, TE = 35 ms, in-plane resolution 2 × 2 mm^2, slice thickness = 2 mm, 1 mm gap) were performed while participants were engaged with the BM task. Stimulus onset intervals were jittered between 4,000 and 8,000 ms in steps of 500 ms, and stimulus order was pseudorandomized, to improve estimation of the event-related response function. In total, 120 stimuli were presented during EPI recording

(60 trials per condition), with a session duration of 456 s each—containing an initial baseline epoch of 24 s, followed by three event-related epochs of 120 s interleaved with three baseline epochs of 24 s. HARDI data [54 axial slices, TR = 7,800 ms, TE = 108 ms, slice thickness = 2.5 mm, matrix size = 88 × 88, field of view = 216 mm; 64 diffusion gradient directions; b value = 2,600 s/mm^2; one volume without diffusion sensitization (b value = 0 s/mm^2) per session] were acquired over two sessions, to improve consistency and sensitivity of diffusion parameter estimation.

Structural and fMRI data were preprocessed and normalized with standard procedures implemented in Statistical Parametric Mapping (SPM12; Wellcome Centre for Human Neuroimaging, Institute of Neurology, UCL, https://www.fil.ion.ucl.ac.uk/spm/) in MATLAB (MathWorks, Inc.). The preprocessed fMRI data were concatenated over both recording sessions, and a GLM was used for statistical analysis of regionally specific effects.

A single regressor modeled stimulus onsets over the concatenated sessions. The stimulus type was represented by a parametric regressor (positive for stimuli containing a point-light walker; negative for walker-absent stimuli). To account for physiological artifacts, six head motion parameters, white-matter and cerebrospinal fluid time series were included as regressors of no interest. The event-related regressors were then convolved with a hemodynamic response function. Data were high-pass filtered (cutoff frequency of 1/256 Hz), and serial autocorrelations were accounted for by an error term modeled as a first-order autoregressive process with a coefficient of 0.2 mixed with white noise. Subsequently, for the contrasts task (positive first regressor) and walker-present trials (positive parametric regressor), individual whole-brain parameter contrast maps were created and submitted to second-level random-effects analyses in the usual way. The resulting statistical parametric maps were thresholded at $P < 0.05$ (FWE whole-brain corrected for multiple comparisons using random field theory), and activation sites were localized with automated anatomical labeling in SPM (122) and the NeuroSynth.org database (ref. 123; neurosynth.org).

The structural connectivity analysis on the HARDI data were conducted with the FMRIB's Diffusion Toolbox within the FMRIB Software Library (FSL5, Oxford Centre for Functional MRI of the Brain, UK, https://fsl.fmrib.ox.ac.uk/fsl/fslwiki). This analysis is presented in detail elsewhere (41). In brief, Bayesian estimation of diffusion parameters obtained by using sampling techniques with modeling of crossing fibers (BEDPOSTX; ref. 65) on individual normalized HARDI data yielded voxel-wise diffusion parameters. These parameters were used in subsequent probabilistic tractography with crossing fibers (PROBTRACKX; ref. 65; step length = 0.5 mm, number of steps = 2,000, number of pathways = 5,000, curvature threshold = 0.2, modified Euler integration) between the network nodes derived from the fMRI analysis. The nodes were introduced as spherical images with the same coordinates and radius as for DCM (see below). Every node was used as seed for tractography to other regions (targets). For every voxel in the seed, PROBTRACKX provided counts of streamlines connecting this voxel to a voxel in a specific target. Averaging these streamline counts per target across all voxels in the seed afforded a measure of structural connectivity. The procedure was repeated for each combination of seeds and targets in every subject until the individual structural adjacency matrices were complete. Of note, due to absent previous evidence for anatomical connectivity between the left lateral cerebellar lobule Crus I and early visual cortex as well as between this cerebellar region and the FFG, structural connectivity between these nodes was not assessed. The fiber pathways were visually inspected to ensure plausibility. As tractography may yield different results based on which node is used as seed and target, for each pair of nodes, an average for the two-way streamline counts was calculated, resulting in a symmetric weighted structural adjacency matrix per subject, further averaged across all participants to create a second-level matrix. These second-level structural connection strengths were used to constrain second-level PEB estimation on the individual DCMs (*SI Appendix*, Fig. S2*B*). For analysis of the FFG-STS fiber pathway trajectory, the individual tractography outputs were thresholded at 5% of the robust intensity range (corresponding to a 95% confidence interval), and the resulting pathways were converted to individual binary maps that were averaged across subjects, yielding a group variability map (Fig. 4*A* and ref. 45).

DCM. The DCM nodes were identified based on the fMRI analysis of regionally specific effects. Given previous results on right-hemispheric predominance in BM processing (27, 124, 125) and crossed cerebro-cerebellar communication (26), the five right cortical regions and the left lateral cerebellar lobule Crus I exhibiting increased BOLD activation for walker-present compared with walker-absent stimuli were included in the DCM. A region in the early visual cortex (OCC) showing increased activation during visual stimulation compared with baseline but without differential activation to BM was also included to accommodate the visual driving input and to assess whether and how early visual cortex is affected by top-down afferents during BM processing.

The group coordinates were used to identify corresponding individual activation maxima (at $P < 0.05$, uncorrected), present in every participant within a maximum distance of 5 mm from the group activation coordinates. Corresponding time series were extracted by computing the first eigenvariate of all activated voxels within an 8-mm sphere centered on each individual maximum. Of note, the time series entering the DCM were prewhitened as per standard SPM preprocessing procedures. This approach ensured that the residuals of the DCM were approximately independent and identically distributed, fulfilling the normality assumptions of the model. Per subject, a one-state, bilinear, and deterministic DCM with mean-centered inputs was specified, with reciprocal connections between all seven nodes, except between the OCC and left cerebellar lobule Crus I, and the FFG and left cerebellar lobule Crus I (in accordance with the structural connectivity analysis). The parametric regressor (walker-present vs. walker-absent trials) was used to modulate all intrinsic (regional self-connections) and extrinsic (between-region) connections. Individual parameters and a second-level model of effective connectivity were estimated with the default SPM12 settings, including a variational Bayes scheme under the Laplace approximation, yielding a multivariate normal density (43, 126). Integration of structural connectivity measures proceeded under the si-PEB approach (41). Bayesian model reduction (43) provided the log-evidences of 405 models representing different mappings from structural connection strength to effective connection probability, in order to determine the optimal constraints on effective connectivity. The second-level PEB and its effective connectivity parameters optimally constrained by structural connectivity were used for subsequent analyses and hypothesis testing.

Bayesian Model Comparison. We used Bayesian model reduction to assess our hypotheses as to specific effects of BM processing on effective connectivity in the network. To this end, we specified models with different modulating effects of BM on effective connectivity in the temporal module, consisting of the MTC, FFG, and STS (factor 1; number of hypotheses, $n = 16$); on effective connectivity between the MTC, FFG, and STS on one side and the insula and IFG on the other (factor 2; $n = 8$); and on top-down connections from the STS, insula, and IFG to OCC (factor 3; $n = 8$). The different hypotheses per factor are illustrated in *SI Appendix*. All possible combinations of these factors within the three hypothesis sets resulted in 1,024 models. Bayesian model reduction was used to assess the evidence for each of these models. For each factor, log-evidences for models based on the same hypotheses were grouped in families, and the evidence for each particular hypothesis was assessed by a family-wise analysis (127). Finally, Bayesian model averaging across all 1,024 models furnished the parameters encoding the modulating effects of BM and their posterior probability.

Psychophysical and Canonical Variate Analysis. The visual sensitivity to BM was assessed with the signal detection theory (42). Participants' responses to each trial were first classified as hits (correct detection of a walker), correct rejections (correct detection of a walker-absent trial), misses (no detection despite walker presence), or false alarms (indication of walker presence in its absence). The hit and false-alarm rates were used to calculate individual and group d-prime values representing the visual sensitivity to BM. A canonical variate analysis examined whether and how individual d-prime values were related to individual modulatory DCM parameters. Nonparametric Mann–Whitney *U* tests were used to determine whether d-prime values and hit rates differed between participant groups with and without significant structural connectivity between the FFG and STS.

ACKNOWLEDGMENTS. We thank Richard S. J. Frackowiak and Alexander N. Sokolov for discussion and valuable advice. We acknowledge technical support by Ric Davis, Jürgen Dax, Chris Freemantle, Bernd Kardatzki, Rachael Maddock, and Liam Reilly, as well as administrative assistance by Marcia Bennett, David Blundred, Kamlyn Ramkissoon, and Daniela Warr. This research was supported by fellowships from the Baasch-Medicus Foundation; the Leenaards Foundation; the Research Committee Fund, Faculty for Biology and Medicine, University of Lausanne, Switzerland; and the European Academy of Neurology (A.A.S.); by a Wellcome Trust Principal Research Fellowship 088130/Z/09/Z (to K.J.F.); and by the Reinhold Beitlich Foundation, the BBBank Foundation, and the German Research Foundation Grant PA 847/22-1 (to M.A.P.). The funders had no role in study design, data collection and analysis, decision to publish, or preparation of the manuscript.

1. Beer JS, Ochsner KN (2006) Social cognition: A multi level analysis. *Brain Res* 1079: 98–105.
2. Frith CD, Frith U (2012) Mechanisms of social cognition. *Annu Rev Psychol* 63: 287–313.
3. Pavlova MA (2012) Biological motion processing as a hallmark of social cognition. *Cereb Cortex* 22:981–995.
4. Blakemore SJ, Decety J (2001) From the perception of action to the understanding of intention. *Nat Rev Neurosci* 2:561–567.
5. de Gelder B, et al. (2010) Standing up for the body. Recent progress in uncovering the networks involved in the perception of bodies and bodily expressions. *Neurosci Biobehav Rev* 34:513–527.
6. Johansson G (1973) Visual perception of biological motion and a model for its analysis. *Percept Psychophys* 14:201–211.
7. Vallortigara G, Regolin L (2006) Gravity bias in the interpretation of biological motion by inexperienced chicks. *Curr Biol* 16:R279–R280.
8. Di Giorgio E, et al. (2017) Filial responses as predisposed and learned preferences: Early attachment in chicks and babies. *Behav Brain Res* 325:90–104.
9. Beauchamp MS, Lee KE, Haxby JV, Martin A (2002) Parallel visual motion processing streams for manipulable objects and human movements. *Neuron* 34:149–159.
10. Bonda E, Petrides M, Ostry D, Evans A (1996) Specific involvement of human parietal systems and the amygdala in the perception of biological motion. *J Neurosci* 16: 3737–3744.
11. Grossman ED, Blake R (2002) Brain areas active during visual perception of biological motion. *Neuron* 35:1167–1175.
12. Howard RJ, et al. (1996) A direct demonstration of functional specialization within motion-related visual and auditory cortex of the human brain. *Curr Biol* 6: 1015–1019.
13. Pelphrey KA, et al. (2003) Brain activity evoked by the perception of human walking: Controlling for meaningful coherent motion. *J Neurosci* 23:6819–6825.
14. Saygin AP, Wilson SM, Hagler DJ, Jr, Bates E, Sereno MI (2004) Point-light biological motion perception activates human premotor cortex. *J Neurosci* 24:6181–6188.
15. Puce A, Perrett D (2003) Electrophysiology and brain imaging of biological motion. *Philos Trans R Soc Lond B Biol Sci* 358:435–445.
16. Grossman ED, Blake R, Kim CY (2004) Learning to see biological motion: Brain activity parallels behavior. *J Cogn Neurosci* 16:1669–1679.
17. Pavlova M, Lutzenberger W, Sokolov A, Birbaumer N (2004) Dissociable cortical processing of recognizable and non-recognizable biological movement: Analysing gamma MEG activity. *Cereb Cortex* 14:181–188.
18. Pavlova M, Lutzenberger W, Sokolov AN, Birbaumer N, Krägeloh-Mann I (2007) Oscillatory MEG response to human locomotion is modulated by periventricular lesions. *Neuroimage* 35:1256–1263.
19. Krakowski AI, et al. (2011) The neurophysiology of human biological motion processing: A high-density electrical mapping study. *Neuroimage* 56:373–383.
20. Peelen MV, Wiggett AJ, Downing PE (2006) Patterns of fMRI activity dissociate overlapping functional brain areas that respond to biological motion. *Neuron* 49: 815–822.
21. Vaina LM, Solomon J, Chowdhury S, Sinha P, Belliveau JW (2001) Functional neuroanatomy of biological motion perception in humans. *Proc Natl Acad Sci USA* 98: 11656–11661.
22. Grossman E, et al. (2000) Brain areas involved in perception of biological motion. *J Cogn Neurosci* 12:711–720.
23. Grèzes J, et al. (2001) Does perception of biological motion rely on specific brain regions? *Neuroimage* 13:775–785.
24. Saygin AP (2007) Superior temporal and premotor brain areas necessary for biological motion perception. *Brain* 130:2452–2461.
25. Freitag CM, et al. (2008) Perception of biological motion in autism spectrum disorders. *Neuropsychologia* 46:1480–1494.
26. Sokolov AA, et al. (2012) Biological motion processing: The left cerebellum communicates with the right superior temporal sulcus. *Neuroimage* 59:2824–2830.
27. Pavlova MA, et al. (2017) "Wrong way up": Temporal and spatial dynamics of the networks for body motion processing at 9.4 T. *Cereb Cortex* 27:5318–5330.
28. Dasgupta S, Tyler SC, Wicks J, Srinivasan R, Grossman ED (2017) Network connectivity of the right STS in three social perception localizers. *J Cogn Neurosci* 29:221–234.
29. Peelen MV, Downing PE (2005) Selectivity for the human body in the fusiform gyrus. *J Neurophysiol* 93:603–608.
30. Schwarzlose RF, Baker CI, Kanwisher N (2005) Separate face and body selectivity on the fusiform gyrus. *J Neurosci* 25:11055–11059.
31. Zeki S (2015) Area V5-a microcosm of the visual brain. *Front Integr Nuerosci* 9:21.
32. Downing PE, Jiang Y, Shuman M, Kanwisher N (2001) A cortical area selective for visual processing of the human body. *Science* 293:2470–2473.
33. Spiridon M, Fischl B, Kanwisher N (2006) Location and spatial profile of category-specific regions in human extrastriate cortex. *Hum Brain Mapp* 27:77–89.
34. Dijkstra N, Zeidman P, Ondobaka S, van Gerven MAJ, Friston K (2017) Distinct top-down and bottom-up brain connectivity during visual perception and imagery. *Sci Rep* 7:5677.
35. Friston KJ, Harrison L, Penny W (2003) Dynamic causal modelling. *Neuroimage* 19: 1273–1302.
36. David O, et al. (2006) Dynamic causal modeling of evoked responses in EEG and MEG. *Neuroimage* 30:1255–1272.
37. Friston KJ (2011) Functional and effective connectivity: A review. *Brain Connect* 1: 13–36.
38. Alaerts K, Swinnen SP, Wenderoth N (2017) Neural processing of biological motion in autism: An investigation of brain activity and effective connectivity. *Sci Rep* 7: 5612.
39. Jack A, Keifer CM, Pelphrey KA (2017) Cerebellar contributions to biological motion perception in autism and typical development. *Hum Brain Mapp* 38:1914–1932.
40. Shultz S, van den Honert RN, Engell AD, McCarthy G (2015) Stimulus-induced reversal of information flow through a cortical network for animacy perception. *Soc Cogn Affect Neurosci* 10:129–135.
41. Sokolov AA, et al. (October 9, 2018) Linking structural and effective brain connectivity: Structurally informed parametric empirical Bayes (si-PEB). *Brain Struct Funct*, 10.1007/s00429-00018-01760-00428.
42. Macmillan NA, Creelman CD (2005) *Detection Theory: A User's Guide* (Lawrence Erlbaum Associates, Mahwah, NJ).
43. Friston KJ, et al. (2016) Bayesian model reduction and empirical Bayes for group (DCM) studies. *Neuroimage* 128:413–431.
44. Penny WD (2012) Comparing dynamic causal models using AIC, BIC and free energy. *Neuroimage* 59:319–330.
45. Ciccarelli O, et al. (2003) From diffusion tractography to quantitative white matter tract measures: A reproducibility study. *Neuroimage* 18:348–359.
46. Bruce C, Desimone R, Gross CG (1981) Visual properties of neurons in a polysensory area in superior temporal sulcus of the macaque. *J Neurophysiol* 46:369–384.
47. Oram MW, Perrett DI (1996) Integration of form and motion in the anterior superior temporal polysensory area (STPa) of the macaque monkey. *J Neurophysiol* 76: 109–129.
48. Jellema T, Maassen G, Perrett DI (2004) Single cell integration of animate form, motion and location in the superior temporal cortex of the macaque monkey. *Cereb Cortex* 14:781–790.
49. Grossman ED, Battelli L, Pascual-Leone A (2005) Repetitive TMS over posterior STS disrupts perception of biological motion. *Vision Res* 45:2847–2853.
50. Gilaie-Dotan S, Bentin S, Harel M, Rees G, Saygin AP (2011) Normal form from biological motion despite impaired ventral stream function. *Neuropsychologia* 49: 1033–1043.
51. Deen B, Koldewyn K, Kanwisher N, Saxe R (2015) Functional organization of social perception and cognition in the superior temporal sulcus. *Cereb Cortex* 25: 4596–4609.
52. Han Z, et al. (2013) Distinct regions of right temporal cortex are associated with biological and human-agent motion: Functional magnetic resonance imaging and neuropsychological evidence. *J Neurosci* 33:15442–15453.
53. Gilaie-Dotan S, Saygin AP, Lorenzi LJ, Rees G, Behrmann M (2015) Ventral aspect of the visual form pathway is not critical for the perception of biological motion. *Proc Natl Acad Sci USA* 112:E361–E370.
54. Billino J, Braun DI, Böhm KD, Bremmer F, Gegenfurtner KR (2009) Cortical networks for motion processing: Effects of focal brain lesions on perception of different motion types. *Neuropsychologia* 47:2133–2144.
55. Thurman SM, Giese MA, Grossman ED (2010) Perceptual and computational analysis of critical features for biological motion. *J Vis* 10:15.
56. Lu H (2010) Structural processing in biological motion perception. *J Vis* 10:13.
57. Taylor JC, Wiggett AJ, Downing PE (2007) Functional MRI analysis of body and body part representations in the extrastriate and fusiform body areas. *J Neurophysiol* 98: 1626–1633.
58. Taylor JC, Roberts MV, Downing PE, Thierry G (2010) Functional characterisation of the extrastriate body area based on the N1 ERP component. *Brain Cogn* 73:153–159.
59. Fairhall SL, Ishai A (2007) Effective connectivity within the distributed cortical network for face perception. *Cereb Cortex* 17:2400–2406.
60. Nguyen VT, Breakspear M, Cunnington R (2014) Fusing concurrent EEG-fMRI with dynamic causal modeling: Application to effective connectivity during face perception. *Neuroimage* 102:60–70.
61. Gschwind M, Pourtois G, Schwartz S, Van De Ville D, Vuilleumier P (2012) White-matter connectivity between face-responsive regions in the human brain. *Cereb Cortex* 22:1564–1576.
62. Pyles JA, Verstynen TD, Schneider W, Tarr MJ (2013) Explicating the face perception network with white matter connectivity. *PLoS One* 8:e61611.
63. Ethofer T, Gschwind M, Vuilleumier P (2011) Processing social aspects of human gaze: A combined fMRI-DTI study. *Neuroimage* 55:411–419.
64. Blank H, Anwander A, von Kriegstein K (2011) Direct structural connections between voice- and face-recognition areas. *J Neurosci* 31:12906–12915.
65. Behrens TE, Berg HJ, Jbabdi S, Rushworth MF, Woolrich MW (2007) Probabilistic diffusion tractography with multiple fibre orientations: What can we gain? *Neuroimage* 34:144–155.
66. Tuch DS, et al. (2002) High angular resolution diffusion imaging reveals intravoxel white matter fiber heterogeneity. *Magn Reson Med* 48:577–582.
67. Pelphrey KA, Carter EJ (2008) Charting the typical and atypical development of the social brain. *Dev Psychopathol* 20:1081–1102.
68. Cavanagh P, Labianca AT, Thornton IM (2001) Attention-based visual routines: Sprites. *Cognition* 80:47–60.
69. Thornton IM, Rensink RA, Shiffrar M (2002) Active versus passive processing of biological motion. *Perception* 31:837–853.
70. Friston K (2010) The free-energy principle: A unified brain theory? *Nat Rev Neurosci* 11:127–138.
71. Friston K (2005) A theory of cortical responses. *Philos Trans R Soc Lond B Biol Sci* 360: 815–836.
72. Bastos AM, et al. (2015) A DCM study of spectral asymmetries in feedforward and feedback connections between visual areas V1 and V4 in the monkey. *Neuroimage* 108:460–475.
73. Auksztulewicz R, Friston K (2015) Attentional enhancement of auditory mismatch responses: A DCM/MEG study. *Cereb Cortex* 25:4273–4283.
74. Gazzaley A, Nobre AC (2012) Top-down modulation: Bridging selective attention and working memory. *Trends Cogn Sci* 16:129–135.

75. Muckli L, et al. (2015) Contextual feedback to superficial layers of V1. *Curr Biol* 25: 2690–2695.
76. Celeghin A, et al. (2017) Intact hemisphere and corpus callosum compensate for visuomotor functions after early visual cortex damage. *Proc Natl Acad Sci USA* 114: E10475–E10483.
77. Van den Stock J, et al. (2014) Neural correlates of body and face perception following bilateral destruction of the primary visual cortices. *Front Behav Neurosci* 8:30.
78. Craig AD (2009) How do you feel–now? The anterior insula and human awareness. *Nat Rev Neurosci* 10:59–70.
79. Ryvlin P, et al. (2006) Nocturnal hypermotor seizures, suggesting frontal lobe epilepsy, can originate in the insula. *Epilepsia* 47:755–765.
80. Chang LJ, Yarkoni T, Khaw MW, Sanfey AG (2013) Decoding the role of the insula in human cognition: Functional parcellation and large-scale reverse inference. *Cereb Cortex* 23:739–749.
81. Chaminade T, Meltzoff AN, Decety J (2005) An fMRI study of imitation: Action representation and body schema. *Neuropsychologia* 43:115–127.
82. Farrer C, Frith CD (2002) Experiencing oneself vs another person as being the cause of an action: The neural correlates of the experience of agency. *Neuroimage* 15: 596–603.
83. Karnath HO, Baier B, Nägele T (2005) Awareness of the functioning of one's own limbs mediated by the insular cortex? *J Neurosci* 25:7134–7138.
84. Heydrich L, Blanke O (2013) Distinct illusory own-body perceptions caused by damage to posterior insula and extrastriate cortex. *Brain* 136:790–803.
85. Sokolov AA, Miall RC, Ivry RB (2017) The cerebellum: Adaptive prediction for movement and cognition. *Trends Cogn Sci* 21:313–332.
86. Pavlova M, Staudt M, Sokolov A, Birbaumer N, Krägeloh-Mann I (2003) Perception and production of biological movement in patients with early periventricular brain lesions. *Brain* 126:692–701.
87. Sokolov AA, Gharabaghi A, Tatagiba MS, Pavlova M (2010) Cerebellar engagement in an action observation network. *Cereb Cortex* 20:486–491.
88. Blake R, Turner LM, Smoski MJ, Pozdol SL, Stone WL (2003) Visual recognition of biological motion is impaired in children with autism. *Psychol Sci* 14:151–157.
89. Klin A, Lin DJ, Gorrindo P, Ramsay G, Jones W (2009) Two-year-olds with autism orient to non-social contingencies rather than biological motion. *Nature* 459: 257–261.
90. Koldewyn K, Whitney D, Rivera SM (2010) The psychophysics of visual motion and global form processing in autism. *Brain* 133:599–610.
91. Kim J, Doop ML, Blake R, Park S (2005) Impaired visual recognition of biological motion in schizophrenia. *Schizophr Res* 77:299–307.
92. Kim J, Norton D, McBain R, Ongur D, Chen Y (2013) Deficient biological motion perception in schizophrenia: Results from a motion noise paradigm. *Front Psychol* 4:391.
93. Okruszek Ł, Pilecka I (2017) Biological motion processing in schizophrenia–Systematic review and meta-analysis. *Schizophr Res* 190:3–10.
94. Yang GJ, et al. (2014) Altered global brain signal in schizophrenia. *Proc Natl Acad Sci USA* 111:7438–7443.
95. Belmonte MK, et al. (2004) Autism and abnormal development of brain connectivity. *J Neurosci* 24:9228–9231.
96. Wang Z, et al. (2016) Prediction of biological motion perception performance from intrinsic brain network regional efficiency. *Front Hum Neurosci* 10:552.
97. Yang D, et al. (2016) Brain responses to biological motion predict treatment outcome in young children with autism. *Transl Psychiatry* 6:e948.
98. Di Giorgio E, et al.; NIDA-Network (2016) Difference in visual social predispositions between newborns at low- and high-risk for autism. *Sci Rep* 6:26395.
99. Sokolov AA, et al. (2014) Recovery of biological motion perception and network plasticity after cerebellar tumor removal. *Cortex* 59:146–152.
100. Kaiser MD, et al. (2010) Neural signatures of autism. *Proc Natl Acad Sci USA* 107: 21223–21228.
101. Tamietto M, de Gelder B (2010) Neural bases of the non-conscious perception of emotional signals. *Nat Rev Neurosci* 11:697–709.
102. de Gelder B (2006) Towards the neurobiology of emotional body language. *Nat Rev Neurosci* 7:242–249.
103. Sokolov AA, Krüger S, Enck P, Krägeloh-Mann I, Pavlova MA (2011) Gender affects body language reading. *Front Psychol* 2:16.
104. Kret ME, Pichon S, Grèzes J, de Gelder B (2011) Men fear other men most: Gender specific brain activations in perceiving threat from dynamic faces and bodies–An FMRI study. *Front Psychol* 2:3.
105. Hubert B, et al. (2007) Brief report: Recognition of emotional and non-emotional biological motion in individuals with autistic spectrum disorders. *J Autism Dev Disord* 37:1386–1392.
106. Vaskinn A, et al. (2016) Reading emotions from body movement: A generalized impairment in schizophrenia. *Front Psychol* 6:2058.
107. Bigelow NO, et al. (2006) Perception of socially relevant stimuli in schizophrenia. *Schizophr Res* 83:257–267.
108. Krüger S, Sokolov AN, Enck P, Krägeloh-Mann I, Pavlova MA (2013) Emotion through locomotion: Gender impact. *PLoS One* 8:e81716.
109. Engelstad KN, Sundet KS, Andreassen OA, Vaskinn A (2017) Body language reading of emotion in schizophrenia: Associations with symptoms and functional outcome. *Scand J Psychol* 58:359–366.
110. Heberlein AS, Saxe RR (2005) Dissociation between emotion and personality judgments: Convergent evidence from functional neuroimaging. *Neuroimage* 28: 770–777.
111. Heberlein AS, Adolphs R, Tranel D, Damasio H (2004) Cortical regions for judgments of emotions and personality traits from point-light walkers. *J Cogn Neurosci* 16: 1143–1158.
112. Alaerts K, et al. (2014) Underconnectivity of the superior temporal sulcus predicts emotion recognition deficits in autism. *Soc Cogn Affect Neurosci* 9:1589–1600.
113. de Haan EH, Cowey A (2011) On the usefulness of 'what' and 'where' pathways in vision. *Trends Cogn Sci* 15:460–466.
114. Mikellidou K, et al. (2017) Area prostriata in the human brain. *Curr Biol* 27: 3056–3060.e3.
115. Tamietto M, Leopold DA (2018) Visual cortex: The eccentric area prostriata in the human brain. *Curr Biol* 28:R17–R19.
116. Sokolov AA, Erb M, Grodd W, Pavlova MA (2014) Structural loop between the cerebellum and the superior temporal sulcus: Evidence from diffusion tensor imaging. *Cereb Cortex* 24:626–632.
117. Willems RM, Peelen MV, Hagoort P (2010) Cerebral lateralization of face-selective and body-selective visual areas depends on handedness. *Cereb Cortex* 20:1719–1725.
118. Goldstein JM, Jerram M, Abbs B, Whitfield-Gabrieli S, Makris N (2010) Sex differences in stress response circuitry activation dependent on female hormonal cycle. *J Neurosci* 30:431–438.
119. Pavlova MA, Sokolov AN, Bidet-Ildei C (2015) Sex differences in the neuromagnetic cortical response to biological motion. *Cereb Cortex* 25:3468–3474.
120. Anderson LC, et al. (2013) Sex differences in the development of brain mechanisms for processing biological motion. *Neuroimage* 83:751–760.
121. Cutting JE (1978) Generation of synthetic male and female walkers through manipulation of a biomechanical invariant. *Perception* 7:393–405.
122. Tzourio-Mazoyer N, et al. (2002) Automated anatomical labeling of activations in SPM using a macroscopic anatomical parcellation of the MNI MRI single-subject brain. *Neuroimage* 15:273–289.
123. Yarkoni T, Poldrack RA, Nichols TE, Van Essen DC, Wager TD (2011) Large-scale automated synthesis of human functional neuroimaging data. *Nat Methods* 8: 665–670.
124. Grosbras MH, Beaton S, Eickhoff SB (2012) Brain regions involved in human movement perception: A quantitative voxel-based meta-analysis. *Hum Brain Mapp* 33: 431–454.
125. Engell AD, McCarthy G (2013) Probabilistic atlases for face and biological motion perception: An analysis of their reliability and overlap. *Neuroimage* 74:140–151.
126. Friston K, Zeidman P, Litvak V (2015) Empirical Bayes for DCM: A group inversion scheme. *Front Syst Neurosci* 9:164.
127. Penny WD, et al. (2010) Comparing families of dynamic causal models. *PLoS Comput Biol* 6:e1000709.